Propulsion and Energy Forum
July 28-30, 2014, Cleveland, OH
50th AIAA/ASME/SAE/ASEE Joint Propulsion Conference

Hall Effect Thruster Electrical Interaction with a Conductive Vacuum Chamber

Jonathan A. Walker[1], Jason D. Frieman,[2] and Mitchell L. R. Walker[3]
Georgia Institute of Technology, Atlanta, Georgia, 30332

Vadim Khayms[4]
Lockheed Martin Space Systems Company, Sunnyvale, California, 94089

Abstract

The goal of this investigation is to characterize the electrical interaction between a Hall effect thruster (HET) and an electrically-conductive vacuum chamber. In order to control the strength of this electrical facility interaction, the cathode radial position with respect to the thruster centerline is varied. The Aerojet-Rocketdyne T-140 laboratory-model HET, operating at 300 V with a discharge current of 10.16 A and a mass flow rate of 11.61 mg/s of xenon, serves as the representative HET test bed. The chamber pressure during operation is 7.3 x 10^{-6} Torr corrected for xenon. Two 0.91-m x 0.91-m square aluminum plates are placed adjacent to, but electrically isolated from, the walls of the electrically-conductive vacuum chamber at two locations: 1) 2.3 m radially outward from thruster centerline centered along the exit plane and 2) 4.3 m axially downstream from the thruster exit plane. The plates are configured in three distinct electrical configurations (grounded, isolated, and connected to each other). The plates serve as a diagnostic that can be used to characterize the chamber-thruster electrical interaction. The HET body was configured in two configurations: electrically floating and electrically grounded. At each plate configuration and thruster body configuration, the radial separation distance between the cathode and the thruster is varied from 18.1 cm to 128.8 cm away from thruster centerline. At each cathode position, the current-to-ground, the floating voltage, and the current conducted between the plates are measured temporally. At each experimental configuration, the thrust, efficiency, and specific impulse are measured. 1-m downstream centerline point measurements of most probable ion energy and plasma potential are achieved with a retarding potential analyzer and emissive probe, respectively Analysis of data point to three separate electron termination paths that govern the thruster-to-chamber coupling.

I. Introduction

THE high specific impulse, thrust efficiency, and thrust density provided by Hall effect thrusters (HETs) makes them an appealing choice for use as the primary propulsion system on board a number of commercial and government Earth-orbiting satellite missions. In addition to the mass savings offered by these performance attributes, developments in in-space power and the growing Western flight heritage portfolio of HETs have also increasingly made them prime candidates for all-electric satellite bus concepts [1].

[1] National Science Foundation Graduate Fellowship, School of Aerospace Engineering, High-Power Electric Propulsion Laboratory, jwalker30@gatech.edu and Student Member AIAA.
[2] National Science Foundation Graduate Fellowship, Graduate Research Assistant, School of Aerospace Engineering, High-Power Electric Propulsion Laboratory; jfrieman3@gatech.edu. Student Member AIAA.
[3] Associate Professor, School of Aerospace Engineering, High-Power Electric Propulsion Laboratory; mitchell.walker@ae.gatech.edu. Associate Fellow AIAA.
[4] Electric Propulsion Architect, Lockheed Martin Space Systems Company; vadim.khayms@lmco.com. Member AIAA.

The growth in interest and popularity of these devices has caused a corresponding proliferation of facilities conducting HET research and testing. Despite the similarities among the devices tested and measurements recorded at each of these facilities, the wide range of facility geometries, sizes, materials, and base pressures makes it difficult for researchers to compare data sets without the inclusion of facility-dependent corrections [2]. It is therefore necessary to develop an understanding of how to quantify facility effects on HET operation and data collection so that facility-dependent testing artifacts can be corrected for and a facility-independent understanding of the actual device performance can be achieved.

Although several investigations into facility effects exist in the literature, most focus on the role of facility backpressure on data collection and device operation. Previous studies have shown that increases in facility pressure result in artificial increases in device thrust and efficiency due to neutral ingestion or entrainment [3–9]. Work has also been conducted linking background pressure to parasitic facility effects caused by resonant charge exchange (CEX) collisions. Specifically, it has been shown that higher facility pressures lead to increased CEX collisions, which, in turn, introduce additional plume components and artificially increase the ion current density measured by Faraday probes in the extremities of the HET plume [3, 10–12]. Azziz *et al* suggest that the relationship between current density and background pressure is linear for all angular positions in the HET plume [13]. This body of experimental evidence on pressure effects is ultimately focused on the development of a process by which to calibrate any vacuum facility in terms of pressure [10].

In addition to being pressure vessels, HET test facilities are almost ubiquitously metallic, and, as such, have finite conductance. Recent work has indicated that chamber conductance plays a significant role in the HET electrical circuit, and, therefore, represents a previously unexplored topic of electrical facility effects [14]. Specifically, it has been shown that the facility walls act as an alternate recombination pathway for plume ions and electrons that have not undergone recombination prior to reaching the facility walls. The completion of the recombination process at the wall as well as the collection of a significant electron current by the facility walls, significantly alters the path of the electrons in the vacuum test facility. Instead of being forced to travel to the HET plume for collisional recombination, the electrons, instead, can travel to the facility wall to be conducted directly to ground. Thus, any process dependent upon the path of the electrons through the plasma (including plasma reactance and resistance) may be significantly different between facility operation and operation on orbit [14–16].

One of the most important processes related to electron motion through the HET plume is cathode coupling as it affects thrust, specific impulse, radiated EMI, and spacecraft-plume interactions [17]. Specifically it has been shown that increases in HET thrust, efficiency, and cathode coupling voltages as well as a reduction in plume divergence angles can be realized by placing the cathode such that it is either internally mounted or aligned with the axial thrust vector and such that the orifice is located within the strong magnetic field close to the thruster body [15–22]. Varying the radial separation of the cathode and the HET away from this inner position has been shown to cause decreased efficiency and increased coupling voltage [15, 16, 21, 22]. Current explanations for these observed relationships between cathode position and cathode coupling voltage relate these trends to the change in plasma impedance realized when moving the cathode orifice through the magnetic field, specifically, across field separatrix surfaces [15, 16]. However, such theories do not fully account for the losses in coupling efficiency observed with increasing cathode separation distance [15, 16]. Furthermore, they were formulated without any knowledge of the role played by the conductive facility walls in affecting the electron path within a test facility.

Without the use of a di-electric chamber or wall insulator material, a way to fully electrically isolate the HET from the vacuum chamber does not yet exist; however, controlling the coupling between the vacuum chamber and the thruster may be possible. The magnetic field of a HET serves the primary purpose of creating a closed azimuthal drift in the discharge channel that allows for ionization and acceleration of the propellant atoms or molecules. In generating this internal magnetic field, an external magnetic field is created that lies outside the thruster body. In a exterior-mounted cathode, the electrons leave the cathode propagate along magnetic field lines until the electrons collide with neutral particles or encounter the thruster's electric field. The electron-neutral collisions contribute significantly to the mobility of these electrons across magnetic field lines, where they terminate either inside the discharge channel or the HET beam. Because of these effects, the cathode position and orientation with respect to this field and the discharge channel can greatly affect the performance and operational characteristics of the thruster.

If we apply this reasoning to the interaction between the thruster and chamber wall, then the external magnetic field should provide pseudo-impedance between the electrons emanating from the cathode and the vacuum chamber facility. This would lead to the conclusion that there should be two distinct regions of behavior regarding the thruster-to-chamber coupling. If the cathode orifice is in a region of where the magnetic field is strong enough to magnetize the electrons sourced from the cathode, then conductance to the chamber is impeded by the field. If the cathode orifice is in a region where the magnetic field strength is not strong enough to magnetize the electrons, then electron conductance to the surrounding grounded facility is un-impeded.

The conclusion of such a scenario would be that increasing the cathode-to-thruster distance should increase the impact of the chamber facility on the thruster's behavior. If the data observed from this experiment corroborated with this trend, then it would be reasonable to believe that cathode position within the magnetic field plays a substantial role in the chamber-thruster electrical coupling.

If changes in the cathode radial position greatly affect the internal plasma processes of the thruster discharge, then it would be impossible to distinguish the effects of the chamber-to-thruster coupling from effects due to changes in the internal processes within the HET discharge channel. Therefore, a fundamental assumption in the formulation of this investigation is that changing the cathode radial position with respect to the thruster will primarily result in changes in the thruster-to-chamber coupling and will not drastically affect the time-averaged performance of the thruster.

This paper experimentally investigates the role of an electrically conductive facility on cathode coupling in a HET discharge. A representative facility test bed with controllable wall bias is created by placing two large square aluminum plates adjacent to, but electrically isolated from, the walls of the vacuum test facility both axially downstream and radially outward from the exit plane of the Aerojet Rocketdyne T-140 HET. In order to assess the impact of the chamber conductance on cathode coupling, measurements of the current conducted through the plates as well as the voltage to which the plates are biased are taken as the plates are electrically isolated, connected, and grounded and as the cathode is moved from a radial separation distance of 18.1 cm to 128.8 cm with respect to thruster centerline. In order to determine the effect of chamber conductance on the plasma plume as well as compare the plume property sensitivity to measurements from previous work on radial cathode positioning, measurements of the plasma potential and most probable ion energy are also taken 1 m downstream along thruster centerline at each cathode position and plate bias.

II. Experimental Apparatus

A. Vacuum Facility

All experiments were performed in Vacuum Test Facility 2 (VTF-2) at the Georgia Institute of Technology High-Power Electric Propulsion Laboratory (HPEPL). A schematic of this facility is shown in Figure 1. VTF-2 is a stainless-steel chamber measuring 9.2 m in length and 4.9 m in diameter. VTF-2 is evacuated to rough vacuum using one 495 CFM rotary-vane pump and one 3800 CFM blower. High-vacuum is achieved using ten liquid nitrogen-cooled CVI TMI re-entrant cryopumps. The cryopump shrouds are fed using the Stirling Cryogenics SPC-8 RL special closed-loop nitrogen liquefaction system detailed by Kieckhafer and Walker [1].

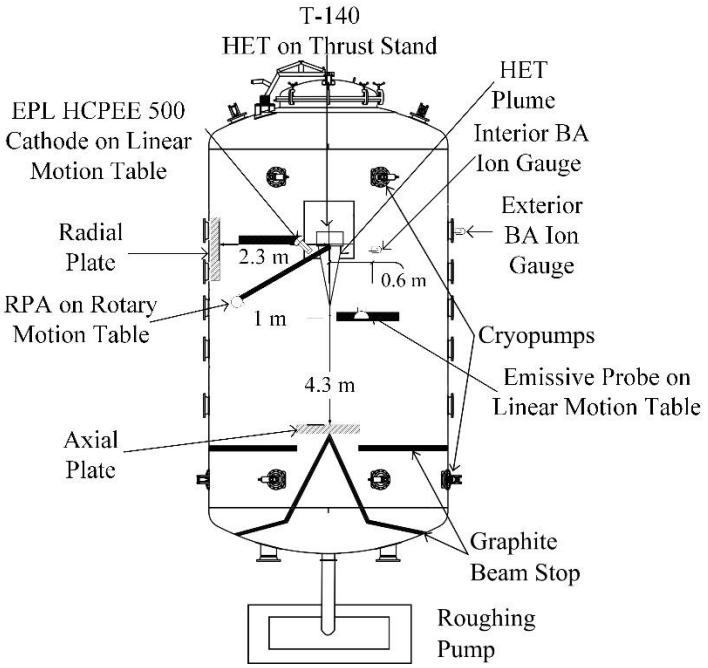

Figure 1 Schematic of VTF-2 and the Layout of the Experimental Apparatus

The facility has a combined nominal pumping speed 350,000 l/s on xenon and can achieve a base pressure of 1.9 × 10^{-9} Torr. Pressure in VTF-2 was monitored using two Agilent BA 571 hot filament ionization gauges controlled by an Agilent XGS-600 Gauge Controller. One gauge was mounted to a flange on the exterior of the chamber while the other was mounted 0.6 m radially outward centered on the exit plane. In order to prevent plume ions from having a direct line of sight to the ionization gauge filament of the interior ion gauge and potentially affecting the pressure measurement, a neutralizer identical to the one used by Walker and Gallimore was attached to the gauge orifice [2]. The nominal operating pressure for this work as measured by the interior and exterior ion gauges were, respectively, 7.3 × 10^{-6} Torr and 1.3 × 10^{-5} Torr +/- 10% corrected for xenon. The corrected pressure (P_c) is found by relating the indicated pressure (P_i) and the vacuum chamber base pressure (P_b) to a gas-specific constant using the following equation [3]:

$$P_c = \left[\frac{P_i - P_b}{2.87}\right] + P_b \tag{1}$$

B. T-140 HET

All experiments detailed in this work were performed using the Aerojet-Rocketdyne T-140 HET originally developed by Space Power, Inc. in collaboration with the Keldysh Research Center and Matra Marconi Space [4]. The T-140 HET is a laboratory-model HET that has a discharge channel made of M26 grade boron nitride with an outer diameter of 143 mm. The performance of the T-140 has been extensively mapped by prior investigations [4]. The thruster body was isolated from facility ground, and thus could be electrically configured as either floating or grounded. Thruster body isolation was achieved via the use of four 1.5 in ceramic stand offs that provides over 1.5 TΩ of electrical isolation at 500 V. For all testing configurations, the thruster was run at 3.1 kW and 300 V at a mass flow rate of 11.61 mg/s of xenon.

An Electric Propulsion Laboratory HCPEE 500-series cathode was located at the 9 o'clock position of the thruster. The cathode flow rate was set to 10% of the anode flow rate for all thruster operating conditions. The orifice location of the cathode was located approximately 2.54 cm downstream of the thruster exit plane at a fixed declination of 55 degrees with respect to the thruster centerline. As shown in Figure 1**,** the radial location of the cathode orifice was varied from 18.1 cm to 128.8 cm outward from the thruster centerline using a Parker Daedal 406XR precision linear motion stage with a 2,000-mm travel. The positional uncertainty of the motion stage is ± 159 μm. The approximate magnetic field strengths at the cathode orifice as a function of radial location away from the thruster centerline are shown in Table 1.

Table 1 Approximate magnetic field strength as a function of cathode orifice radial location away from thruster centerline

Radial Location (cm)	Magnetic Field Strength (G)
18.1	30
19.4	20
20.6	20
21.9	10
24.4	0

The magnetic circuit configuration of the T-140 HET (two concentric coils centered on the thruster centerline) restricts the position of the magnetic field separatrix to the thruster centerline and precludes the T-140 HET from exhibiting the off-centerline separatrix surfaces shown in HETs with magnetic coils centered off-axis [5, 6]. This magnetic field topology eliminates any concerns from this work about the changing nature of the near-field plume properties and cathode coupling as a function of cathode position relative to the absent off-centerline separatrix surface [5].

The T-140 HET discharge was controlled using a Magna-Power TSA800-54 power supply. All other thruster components were powered using TDK-Lambda GEN60-25 power supplies. A TDK-Lambda GEN150-10 and GEN40-38 were used for the cathode keeper and heater, respectively. To protect the discharge supply from thruster oscillations, the discharge supply was connected to a discharge filter consisting of a 95 μF capacitor and a 1.3 Ω resistor in order attenuate discharge current oscillation constitutes greater than 1.4 kHz.

The discharge current oscillations of the T-140 HET were recorded using a Teledyne LeCroy CP150 current probe connected to a Teledyne LeCroy HDO6104 oscilloscope. The uncertainty and bandwidth of the current probe are ± 1% and 10 MHz; for the oscilloscope, they are ± 0.5% full scale and 1 GHz. In the floating thruster body configuration, the thruster body floating voltage was measured differentially using Teledyne LeCroy PP018 passive probes with a bandwidth of 500 MHz and accuracy of ± 0.5% connected to the Teledyne LeCroy oscilloscope. When the thruster body was grounded, the current conducted through the thruster body to ground was measured using a Teledyne LeCroy CP030 current probe connected to the Teledyne LeCroy oscilloscope. The CP030 has a bandwidth of 50 MHz and an accuracy of ± 1%.

The mean discharge voltage of the T-140 HET was measured differentially using a pair of Teledyne LeCroy PPE2kV 100:1 high-voltage probes connected to a Tektronix TDS3034B oscilloscope. The bandwidth of the voltage probes is 400 MHz; the oscilloscope has an uncertainty and bandwidth of ± 2% and 300 MHz. The cathode-to-ground voltage was measured differentially using Tektronix P6139A connected to the Tektronix oscilloscope, which have a bandwidth of 500 MHz and an accuracy of ± 0.5%.

High purity (99.9995%) xenon propellant was supplied to the thruster and cathode using stainless-steel lines metered with MKS 1179A mass flow controllers. The controllers were calibrated before each test day by measuring gas pressure and temperature as a function of time in a known control volume. The mass flow controllers have an uncertainty of ± 0.03 mg/s (5.1%) for the cathode flow and ± 0.12 mg/s (2%) for the anode flow [7].

C. Configuration of Plates

In order to simulate a metallic facility with controllable wall bias, two 0.91 m x 0.91 m x 0.16 cm thick square aluminum plates were mounted adjacent to, but electrically isolated from, the walls of the vacuum test facility. The axial plate was located 4.3 m downstream from the exit plane of the thruster. The radial plate was located 2.3 m radially outward from the thruster centerline and centered on the exit plane of the T-140 HET. Figure 1 shows the physical location of the plates with respect to the T-140 HET. Identical plates have been used in previous studies of electrical facility effects [8].

Figure 2 shows each of the three plate electrical configurations used in this test. In all three cases, the electrical connection to the plates was made using a RG-58 coaxial cable with a grounded shield that passed through a BNC feedthrough into the chamber. This transmission line is similar in style to those previously used to study discharge oscillations in HETs [9, 10].

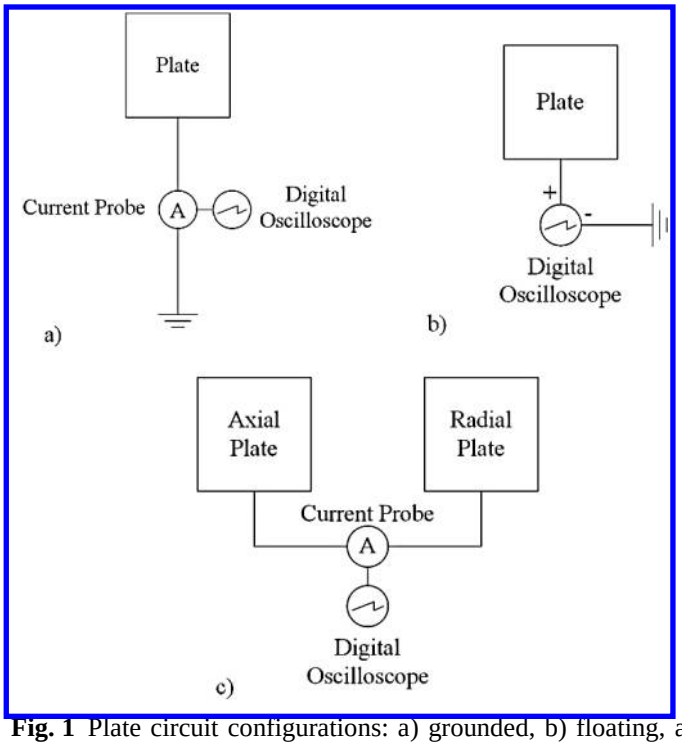

Fig. 1 Plate circuit configurations: a) grounded, b) floating, and c) connected.

In configuration A (grounded), each plate was directly connected to chamber ground with the current conducted between each plate and ground measured with a Teledyne LeCroy CP030 current sensor connected to a Teledyne LeCroy HDO6104 oscilloscope; the plate currents and thruster telemetry signals were measured simultaneously at a sampling frequency of 125 MS/s for a 20 ms window to ensure that multiple fundamental discharge current mode periods were captured. A In configuration B (floating), the plates were electrically isolated, and the floating voltage was measured directly using a Teledyne LeCroy PP018 passive probe to the Teledyne LeCroy oscilloscope; these voltage measurements were also taken simultaneously with measurements of the T-140 HET discharge current and voltage oscillations at a sampling frequency of 125 MS/s. In configurations A and B both plates were simultaneous grounded or floated, respectively. In configuration C (connected), the plates were connected to each other instead of to ground, and the current conducted between the two plates was measured with a Teledyne LeCroy CP030 current probe connected to the Teledyne LeCroy oscilloscope; the current conducted between the two plates and the discharge current were measured simultaneously at a sampling frequency of 125 MS/s.

D. Thrust Stand

Thrust is measured using the null-type, water-cooled, inverted pendulum thrust stand of NASA Glenn Research Center design detailed in the work of Xu and Walker [11]. The thrust stand consists of a pair of parallel plates connected by a series of four flexures that support the top plate and permit it to deflect in response to an applied force. The position of the upper plate is measured using a linear voltage differential transformer (LVDT) and is controlled using two electromagnetic actuators. During operation, the current through each actuator is controlled using a pair proportional-integral-derivative (PID) control loops that use the LVDT signal as input and then modulate the current through the actuators in order to remove any vibrational noise (damper coil) and hold the upper plate stationary (null coil). The thrust is correlated to the resulting current through the null coil required to keep the upper plate stationary. The null coil current is recorded using a Cole-Parmer 200-mm flatbed recorder. The thrust stand is constructed primarily of aluminum and is surrounded by a water-cooled copper shroud in order to maintain thermal equilibrium.

The thrust stand is calibrated by loading and off-loading a set of known weights that span the full range of expected thrust values. A linear fit is then created in order to correlate null coil current to force applied to the thrust stand. The thruster is shut down and a recalibration is performed every 40-60 minutes in order to minimize thermal

drift of the zero position. In order to ensure the thruster is at thermal equilibrium, a warm-up period of 3 hours is taken before thrust measurements begin. During this warm-up period, the thruster is run at the nominal condition of 3.1 kW. The thrust stand uncertainty for this work was ±3 mN (±1.7% full scale).

E. Plume Diagnostics

Because of the large number of individual testing conditions, each of the following plume diagnostic measurements were taken only once at 1 m downstream of the exit plane and at the thruster centerline. In this way, the general trends of the beam plasma can be measured. The emissive probes are mounted on a linear stage located 1 m downstream from the thruster as shown in Figure 1. The spacing between the probes is kept at 16.51 cm to mitigate the sheath interaction between the probes. To reduce beam exposure time on the retarding potential analyzer (RPA), the diagnostic is mounted to a 1 m long boom capable of sweeping a 180° arc around the thruster.

1. Emissive Probe

The emissive probe is constructed of a loop of 0.005" diameter 2% Thoriated-Tungsten filament housed in a double bore alumina tube. Despite the relatively small diameter of filament, probe lifetimes in excess of 8 hours were observed using a low emission current type of method as mentioned in Sheehan and Hershkowitz [34]. Probe currents of 1.2 A at beginning of probe life to 1.8 A at end of probe life produced the inflection point in the voltage characteristic of the probe. In this method, the probe is heated and then the emission current is monitored as the probe bias is swept in a manner similar to that used with Langmuir probes. The changing characteristic of the emission current trace as a function of applied bias voltage is then used to determine the plasma potential. The heating current to the emissive probe filament was varied from 1.87 A to 1.91 A using a Xantrex XPD 60-9 power supply. A Keithley 2410 1100 V sourcemeter was used to control the probe circuit bias and the probe emission current was measured using a Keithley 6485 Picoammeter. At each operating condition, one bias sweep was taken per heating current. During each bias sweep, the probe voltage was varied over a range of 0-250 V in 1 V increments with a 300 ms dwell time. The Sourcemeter and Picoammeter were simultaneously controlled using a LabView Virtual Instrument to ensure synchronous recording of the probe bias voltage and emitted current.

The inflection point was then found in each of the I-V traces for each of the different heating current levels, and the plasma potential was found by linearly extrapolating these values to zero emission. Due to the low density plasma environment, these results were confirmed using the separation technique to ensure accuracy [34].

2. Retarding Potential Analyzer

The ion energy distribution in the thruster plume was measured using a retarding potential analyzer (RPA). The RPA is a well-known diagnostic that uses a set of electrostatically biased grids to act as a high-pass energy filter and selectively filter ions based on the ion energy [31, 32]. For this work, the four grid RPA design similar to the one previously used by Xu was used [33]. The grids are (in order from the plasma from the collector): the floating grid, the electron repulsion grid, the ion repulsion grid, and the electron suppression grid. The floating grid is allowed to float to the plasma potential in order to shield the plasma from perturbations caused by the presence of the probe. The electron repulsion grid is biased negative relative to ground in order to prevent plasma electrons from reaching the collector. The electron suppression grid is similarly biased in order to repel any secondary electrons created within the probe. The ion repulsion grid is biased positive relative to ground in order to impede the motion of the incident ions, and thus filter the ion population based upon directed kinetic energy.

In this work, the electron suppression and repulsion grids were both biased to -30 V using two TDK-Lambda GENH 60-12.5 power supplies. The ion repulsion grid bias, swept from 0 V to 450 V, was controlled by a Keithley 2410 Sourcemeter and the collector current was measured using a Keithley 6487 Picoammeter. The grids have a 2.286 cm collection diameter and 31% open area. To prevent the RPA from overheating, the RPA is attached to a rotary arm and is able to swing to the same position emissive probe measurements as illustrated in Figure 1. RPA data were collected only on centerline, 1 m downstream from the exit plane of the T-140 HET. The variability in the RPA measurement between sweeps of the same condition were +/- 10%.

III. Results

A. Time-Average Plate and Thruster Current and Voltages

The cathode-to-ground voltage shown in Figure 2 show three distinct regions of behavior: Region 1, the cathode-to-ground voltage remains constant, Region 2, the cathode-to-ground voltage decreases in magnitude, and Region 3, the cathode-to-ground voltage begins to decrease in magnitude. The physical underpinning for this regional delineation is described in greater detail in the Discussion section.

As the cathode outwards from the nominal position, the time averaged values of the radial and axial plate electrical and thruster body-to-ground current reveal three distinct regions of behavior. The clearest indicator of these regions, the thruster body floating voltage, is shown in Figure 3. Figure 4 shows the time average currents for the plate and thruster diagnostics. The trends in this figure also commiserate with behavior shown in the floating voltages.

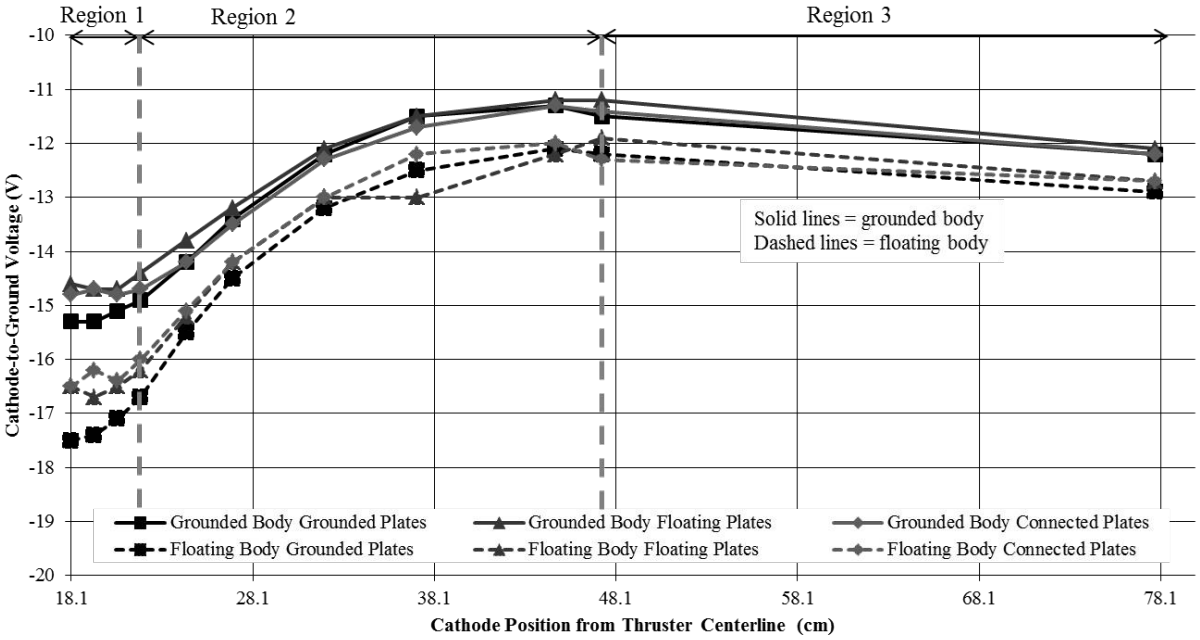

Figure 2 Cathode to GND voltage of the HET taken at 300V, 3.1 kW

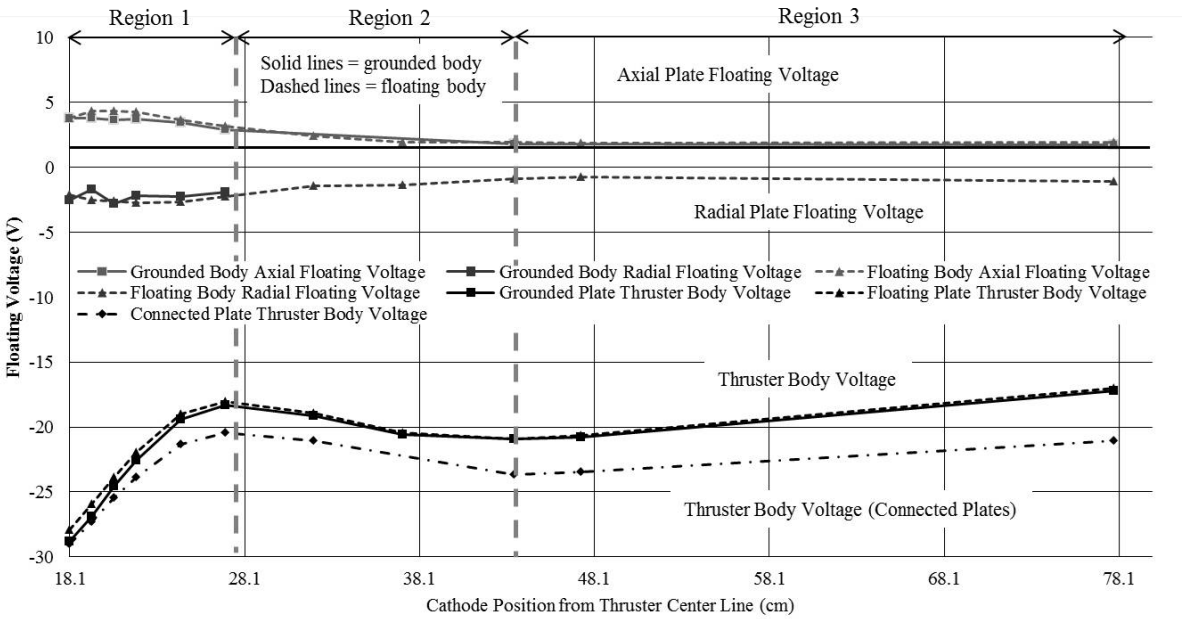

Figure 3 The floating voltages for the radial plate, axial plate, and the thruster body floating voltage for the floating type configurations. HET conditions are at 300 V, 3.1 kW.

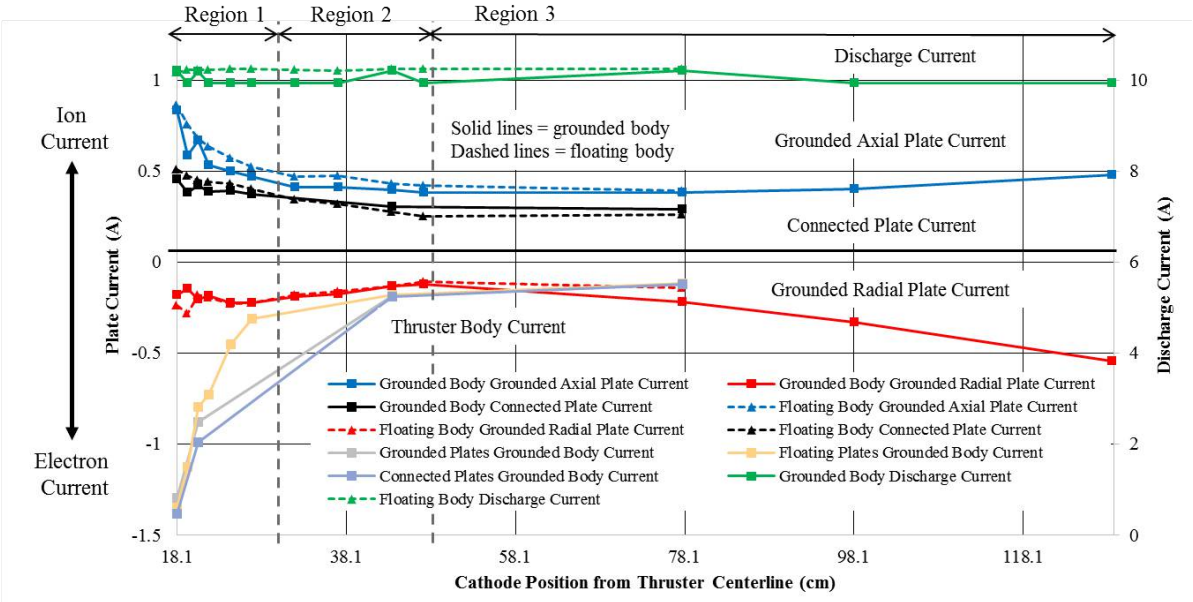

Figure 4 The radial plate, axial plate, and thruster body current to ground as a function of cathode position for connected and grounded configurations. HET nominal conditions are at 300V, 3.1 kW

Looking at Figure 2, the sign of the current to ground reveals the nature of the kind of current collected. As a matter of convention, positive current is in the direction of positive charge movement. A negative current indicates a collection of electrons and a positive current indicates a collection of ions. The radial plate and the thruster body current and voltage trends indicate an electron dominated plasma environment, whereas the axial plate indicates an ion dominated plasma environment. This conclusion makes sense intuitively as the radial and thruster body region is

dominated by energetic cathode electrons and low energy charge exchange ions and the axial plate region lies at the center of the beam and is dominated by highly energetic beam ions.

B. Plume Diagnostics

1. *Plasma Potential*

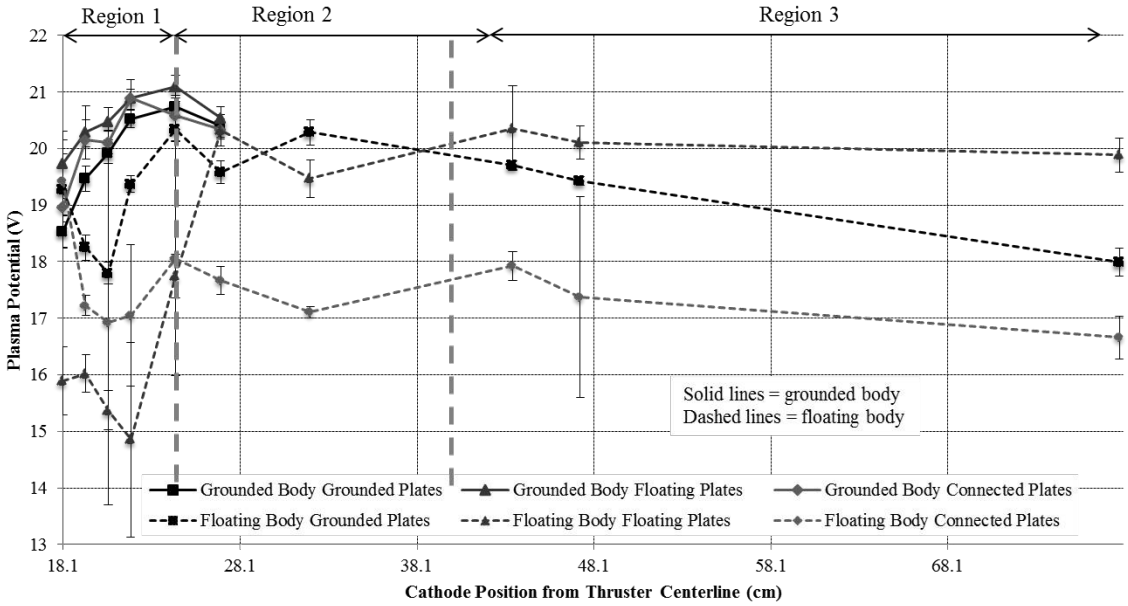

Figure 5 Plasma potential measurements taken at thruster centerline at 1 m downstream.

2. *Most Probable Ion Energy*

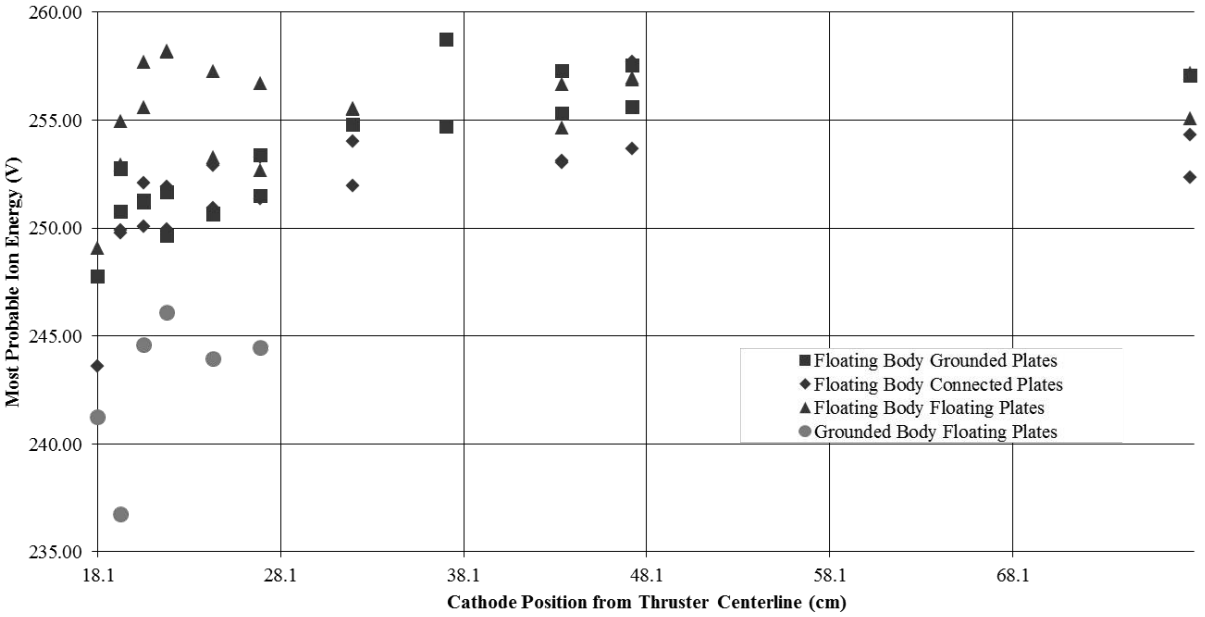

Figure 6 Retarding Potential Analyzer results take at thruster centerline at 1 m downstream. RPA measurement variability is +/- 10%

C. Thrust Measurements

Figure 7 and Figure 8 show the thrust measurements for the various experimental configurations. The changes expected in thrust due to cathode radial position are expected to be less than that variability. To overcome this

limitation, thrust measurements are taken consecutively with a spacing of 2 minutes between cathode radial positions. This means that between plate and thruster body configurations, the variability is still 3.4%, but at least the changes for a given plate configuration can be observed with less than 1% uncertainty.

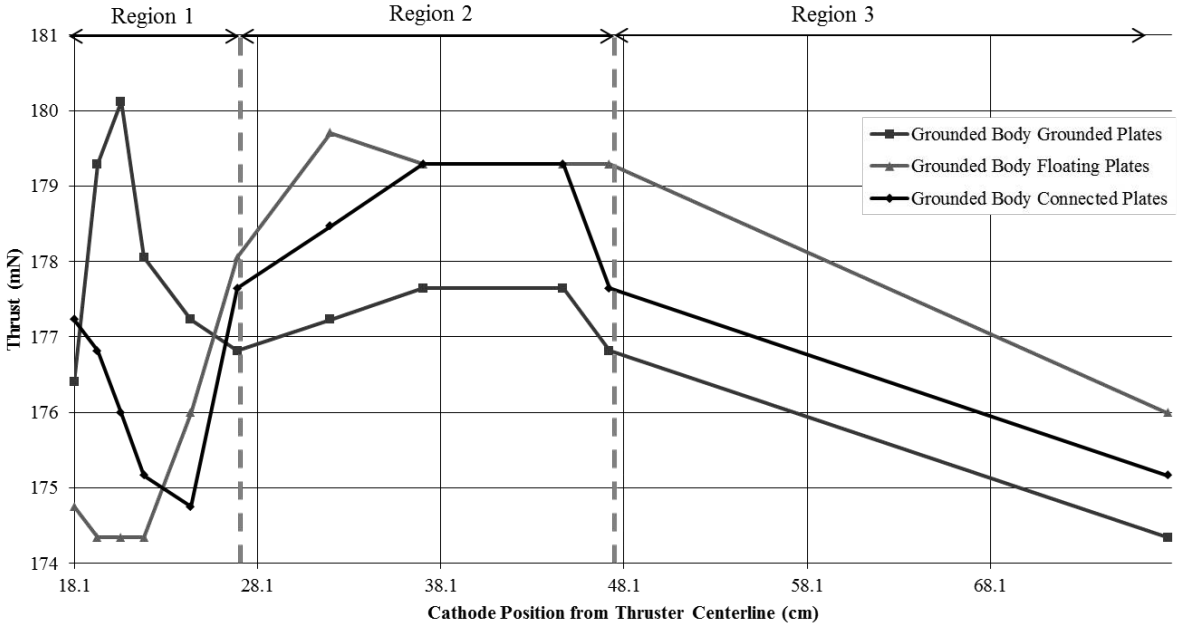

Figure 7 Grounded thruster body configuration. The absolute uncertainty +/- 1.7%. The variability between cathode positions, (i.e. relative uncertainty) for a given plate configuration is less than 1%.

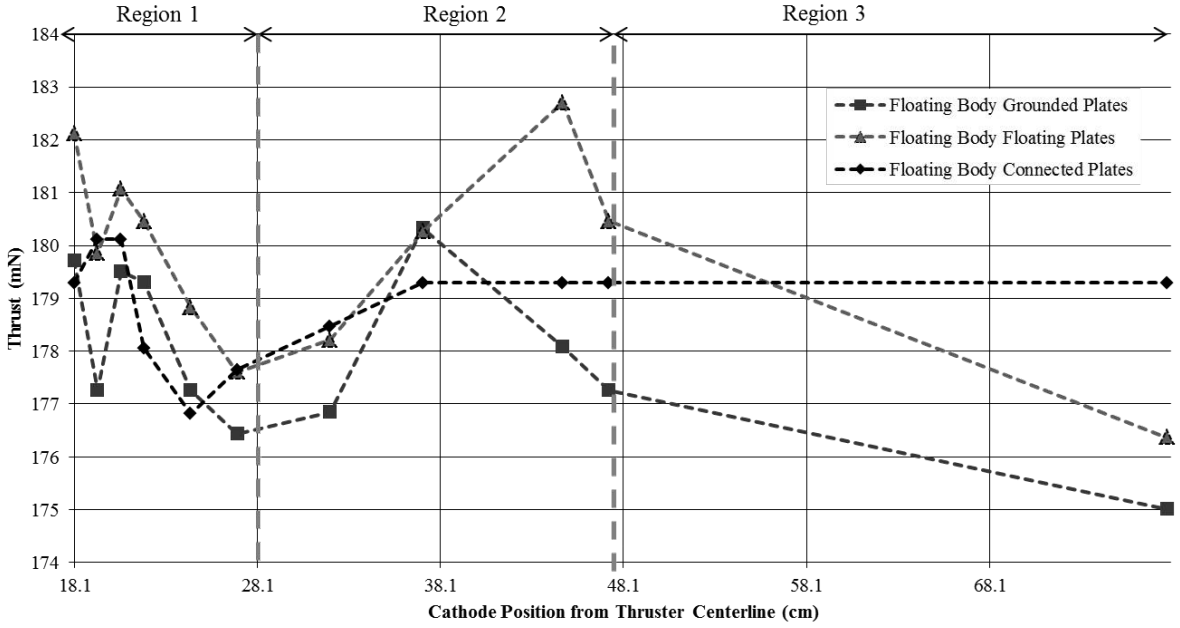

Figure 8 Floating thruster body configuration. The variability between plate configurations is +/- 3%. The variability between cathode positions for a given plate configuration is less than 1%.

D. Waveform Frequency Power Spectrum

For each plate and thruster configuration tested, the radial plate, axial plate, and discharge current waveforms were captured simultaneously at 125 MS/s for a length of 20 ms. The DC signal from the waveforms were removed by subtracting out the average voltage or current over the 20 ms capture length. A Fast Fourier Transform (FFT) was applied using MATLAB to the data to obtain the frequency power spectrum. The spectral resolution at that sample

rate is 12 Hz and the spectral bandwidth, including probe bandwidth, is 5 MHz. The frequency component of the discharge current and the radial plate current power spectrum with the most power is plotted against cathode position as shown in Figure 9 and Figure 10 respectively.

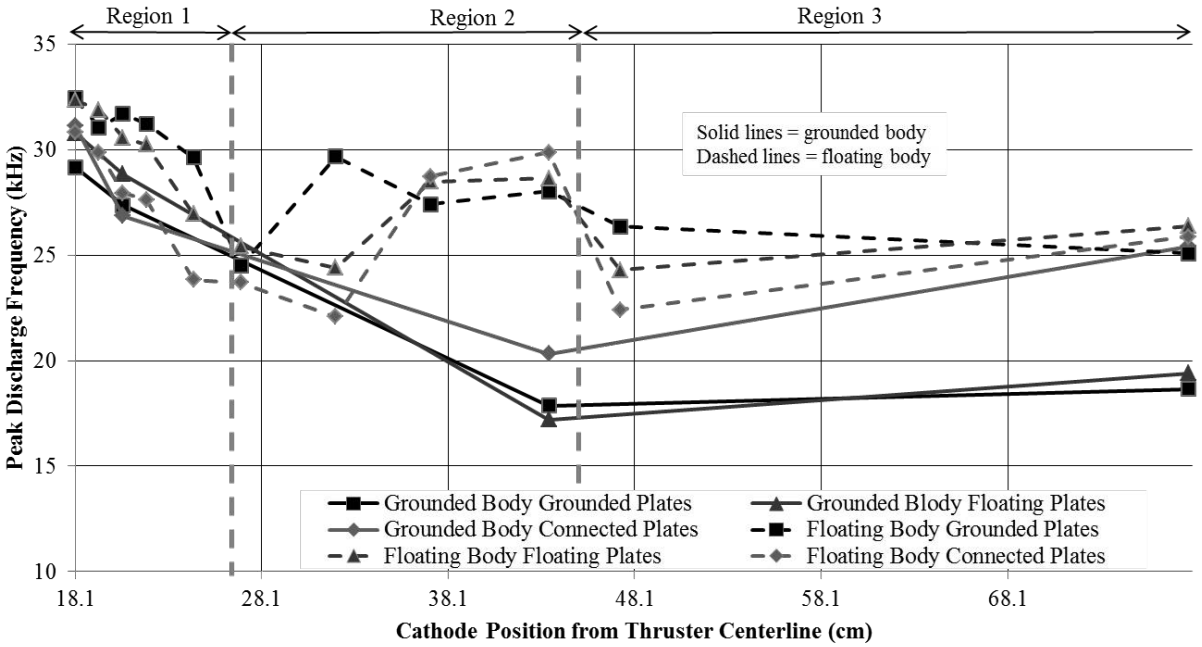

Figure 9 Peak discharge current FFT frequency as a function of cathode position

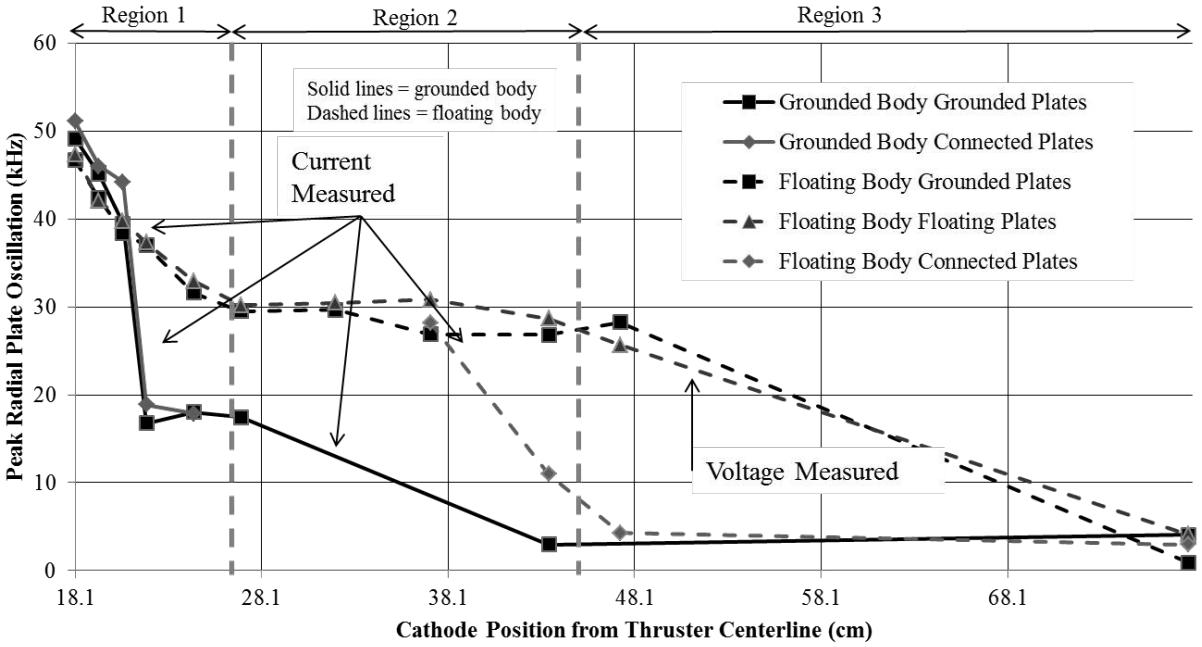

Figure 10 Peak Radial Plate current or voltage FFT frequency as a function of cathode position

IV. Discussion

Based on the results shown in the previous section, there is indeed evidence of thruster-to-chamber electrical coupling and this coupling is dependent on the position of the cathode. To fully understand the extent of this coupling, the nature of this coupling, and the physical processes governing the thruster to chamber electrical coupling must be examined.

A. Cathode Position Impact on Internal Discharge Plasma Mechanisms

Figure 7 and Figure 8 reveal that the thrust produced is dependent on the cathode position. The variation is as high as a 3% increase in thrust relative to the nominal cathode position across all thruster and plate configurations. For each configuration, as shown in the Figure 7, the thrust measurements are taken within 2 minutes. Therefore, those changes measured in thrust can be considered outside the variability of the measurement. From first principles, the thrust should scale with the square root of the acceleration potential of the thruster. Therefore, the observed changes in plasma potential and cathode-to-ground voltage as shown in Figure 2 and Figure 5 can account fully for the observed variation in thrust. The RPA data displayed in Figure 6 shows variability in the most probable ion energy within the error of the RPA. This measurement is corrected for changes in the plasma potential. From a time-averaged behavior standpoint, the insensitivity of the most probably ion energy to the cathode position strongly suggests that the ionization and acceleration processes within the thruster remain largely unaffected by the change in the cathode position. This makes sense intuitively as the acceleration potential depends primarily on factors that remain constant throughout the experiment. Because the changes in thrust measured can be accounted for by changes in the acceleration voltage, it is reasonable to say, from a time-averaged perspective, that the HET internal discharge plasma behavior remains largely insensitive to cathode radial position.

B. Electron Termination Pathways

In Figure 3 and Figure 4, the radial plate and axial plate electrical waveforms show three distinct regions of behavior with respect to cathode distance to the thruster centerline. These regional divisions propagate throughout the plasma potential, thrust, cathode-to-ground, and thruster body current or voltage data. Therefore, in order to understand the behavior shown in Figure 3 and Figure 4, we must first consider what constituents of the plasma drive the coupling between the chamber plates and the thruster. Between the thruster and the chamber plates, radial and axial, there exists a plasma environment created by the thruster or beam related physical processes. The axial direction coupling behavior is driven by the kinetic behavior of the thruster acceleration, and the radial direction coupling behavior is driven by cathode-originated electrons. This makes sense as the downstream plasma is the most-dense and primary composed of beam ions, and the radial direction plasma is primarily a charge-exchange plasma environment. The key to understanding the behavior shown in the data is to determine where the electrons generated by the cathode are terminating. In the static picture of HET operation, there are only the electrons sourced from the cathode for ionization that terminate at the anode and neutralization that terminate in the beam. As illustrated in the Results section, the picture is more complicated and the axial and radial plate collected current behavior points towards three plausible preferred electron termination pathways that give rise to three regions of behavior.

In Region 1, the electrons preferentially terminate through the grounded thruster body and nearby grounded surfaces. As shown in Figure 4, the thruster body collected current is highest in magnitude out of all the regions and the sign is negative, which correlates to collected electron current. In Region 1, the cathode is still well within the thruster magnetic field and the electrons are still highly magnetized, i.e. the electron hall parameter is much greater than 1. Therefore, electrons generated by the cathode are effectively trapped within the HET external magnetic field. The thruster body floating voltage is also the most negative in Region 1, which also suggests an increased electron density near the thruster body. In terms of the thruster body preferential electron termination argument, the most convincing of the data collected is the peak frequency components of the discharge current. When the cathode is in Region 1 locations, the peak frequency of the discharge, as shown in Figure 9, is the highest in frequency, which suggests that the enhanced electron termination to the thruster can support high frequency modes of oscillations as compared to the other cathode regions. In Regions 2 and 3, the discharge current peak frequency drops by approximately 10 kHz. The data collected through the plate mean currents and the discharge current oscillations point to Region 1 being governed by a preferred electron termination pathway into the thruster body.

Region 2 corresponds to a preferred electron termination pathway into the beam. In this region, the electrons range from being weakly to no longer magnetized, i.e. the electron hall parameter is on the order of unity. In Figure 4, the axial collected ion current begins to decrease as more electrons are being terminated into the beam. This would correspond to better ion-electron recombination in the plume and fewer ions reaching the axial plate. The

grounded thruster body current and the floating thruster body voltage both show a decrease in magnitude as compared to the other regions suggesting electrons are no longer preferentially terminating on the thruster body. The Region 2 electron termination pathway into the beam is supported heavily by the trends showing a decrease in plasma potential as shown in Figure 5.

Finally in Region 3, the cathode is outside the influence of the thruster magnetic field, and the electron hall parameter is much less than unity. The primary electron termination pathway is the radial plate. The radial plate current shown in Figure 4 is the highest in Region 3. In this region, there is a shift in the fundamental coupling mechanism to the radial plate. In Region 1 and Region 2, the peak frequency of the discharge current oscillations appear as peak frequencies in the radial plate FFT, as shown in Figure 9 and Figure 10. In Region 3 cathode locations, the peak radial plate oscillation frequency is in the sub 5 kHz regime, while the thruster discharge current peak frequency is in the 20 kHz regime. The Region 3 radial plate current also shows peaks in the frequency range corresponding to thruster breathing/spoke mode, but the sub 5 kHz peak is 10-15 dB stronger than this breathing mode peak. This would indicate a fundamental shift in the dominant coupling mechanism. An estimate for the electron-neutral collision rate in the region between the cathode and the radial plate reveals a collision frequency on the order 1-2 kHz, making the electron-neutral collisions in the charge exchange plasma near the radial plate the primary driver for the Region 3 thruster-to-radial chamber plate coupling.

In summary, the data heavily supports three electron termination pathways: Region 1, thruster-to-facility coupling is driven by electron termination into the thruster body or close-by grounded surfaces, Region 2, thruster to facility coupling is driven by electron termination into the beam, and Region 3, thruster to facility coupling is driven by electron termination into the radial walls of the chamber.

V. Conclusion

The thruster-to-chamber electrical interaction is driven by where the cathode-originated electrons terminate. Those electron termination pathways govern not only plume characteristics of the HET, but also the discharge current oscillations. The findings of this investigation only further underline the importance of characterizing the ground-based testing facility's interaction with the HET and provides some new insights, through the electron termination pathways, on how the HET electrically interacts with its testing environment.

VI. Acknowledgement

J.A. Walker would like to thank the National Science Foundation Graduate Research Fellowship Program for funding that enabled this research to be accomplished.

VII. References

[1] D. Goebel, M. Martinez-Lavin, T. Bond, and A. King, "Performance of XIPS Electric Propulsion in On-orbit Station Keeping of the Boeing 702 Spacecraft," *38th AIAA/ASME/SAE/ASEE Joint Propulsion Conference & Exhibit*, Jul. 2002.

[2] A. Semenkin, V. Kim, O. Groshkov, and R. Jankovsky, "Development of Electric Propulsion SStandard-Current Status and Further Activity," in *Proceedings of the 27th International Electric Propulsion Conference*, 2001, no. IEPC Paper 2001–070.

[3] D. Brown and A. Gallimore, "Evaluation of Plume Divergence and Facility Effects on Far-Field Faraday Probe Current Density Profiles," in *Proceedings of the 31st International Electric Propulsion Conference*, 2009, no. IEPC-2009–030.

[4] K. Diamant, R. Spektor, E. Beiting, J. Young, and T. Curtiss, "The Effects of Background Pressure on Hall Thruster Operation," *48th AIAA/ASME/SAE/ASEE Joint Propulsion Conference & Exhibit*, Jul. 2012.

[5] D. M. Goebel and I. Katz, *Fundamentals of Electric Propulsion: Ion and Hall Thrusters*. Wiley, 2008.

[6] R. Hofer, P. Peterson, and A. Gallimore, "Characterizing Vacuum Facility Backpressure Effects on the Performance of a Hall Thruster," in *Proceedings of the 27th International Electric Propulsion Conference*, 2001, no. IEPC-01–045.

[7] M. R. Nakles and W. A. Hargus, "Background Pressure Effects on Ion Velocity Distribution Within a Medium-Power Hall Thruster," *Journal of Propulsion and Power*, vol. 27, no. 4, p. 737â€“743, Jul. 2011.

[8] T. Randolph, V. Kim, H. Kaufman, K. Kozubskii, V. Zhurin, and M. Day, "Facility Effect on Stationary Plasma Thruster Testing," in *Proceedings of the 23rd international Electric Propulsion Conference*, 1993, no. IEPC-93–093.

[9] B. M. Reid, "The Influence of Neutral Flow Rate in the Operation of Hall Thrusters," University of Michigan, 2009.

[10] M. L. R. Walker, "Effects of Facility Backpressure on the Performance and Plume of a Hall Thruster," University of Michigan, Ann Arbor, MI, 2005.

[11] M. Walker, R. Hofer, and A. Gallimore, "The Effects of Nude Faraday Probe Design and Vacuum Facility Backpressure on the Measured Ion Current Density Profile of Hall Thruster Plumes," in *38th AIAA/ASME/SAE/ASEE Joint Propulsion Conference & Exhibit*, 2002.

[12] M. L. R. Walker, A. L. Victor, R. R. Hofer, and A. D. Gallimore, "Effect of Backpressure on Ion Current Density Measurements in Hall Thruster Plumes," *Journal of Propulsion and Power*, vol. 21, no. 3, pp. 408–415, 2005.

[13] Y. Azziz, M. Martinez-Sanchez, and J. Szabo, "Determination of In-Orbit Plume Characteristics from Laboratory Measurements," in *42nd AIAA/ASME/SAE/ASEE Joint Propulsion Conference & Exhibit*, 2006.

[14] J. D. Frieman, S. T. King, M. L. R. Walker, V. Khayms, and D. King, "Role of a Conducting Vacuum Chamber in the Hall Effect Thruster ElElectric Circuit," 2014.

[15] J. D. Sommerville and L. B. King, "Hall-Effect Thruster–Cathode Coupling, Part II: Ion Beam and Near-Field Plume," *Journal of Propulsion and Power*, vol. 27, no. 4, p. 754â€"767, Jul. 2011.

[16] J. D. Sommerville and L. B. King, "Hall-Effect Thruster–Cathode Coupling, Part I: Efficiency Improvements from an Extended Outer Pole," *Journal of Propulsion and Power*, vol. 27, no. 4, p. 744â€"753, Jul. 2011.

[17] D. Tilley, K. de Grys, and R. Myers, "Hall thruster-cathode coupling," *35th Joint Propulsion Conference and Exhibit*, Jun. 1999.

[18] L. Albarede, V. Lago, P. Lasgorceix, M. Dudeck, A. I. Bugrova, and K. Malik, "Interaction of a Hollow Cathode Stream with a Hall Thruster," in *Proceedings of the 28th International Electric Propulsion Conference*, 2003, no. IEPC Paper 2003–333.

[19] R. Hofer, L. Johnson, D. Goebel, and D. Fitzgerald, "Effects of an Internally-Mounted Cathode on Hall Thruster Plume Properties," *Proceedings of the 42nd AIAA/ASME/SAE/ASEE Joint Propulsion Conference & Exhibit*, Jul. 2006.

[20] K. K. Jameson, D. Goebel, R. Hofer, and R. M. Watkins, "Cathode Coupling in Hall Thrusters," in *Proceedings of the 30th International Electric Propulsion Conference*, 2007, no. IEPC Paper 2007–278.

[21] J. Sommerville and L. King, "Effect of Cathode Position on Hall-Effect Thruster Performance and Cathode Coupling Voltage," *43rd AIAA/ASME/SAE/ASEE Joint Propulsion Conference & Exhibit*, no. AIAA 2007–5174, Jul. 2007.

[22] M. L. R. Walker and A. D. Gallimore, "Hall Thruster Cluster Operation with a Shared Cathode," *Journal of Propulsion and Power*, vol. 23, no. 3, pp. 528–536, May 2007.

[23] A. Kieckhafer and M. L. R. Walker, "Recirculating Liquid Nitrogen System for Operation of Cryogenic Pumps," in *Proceedings of the 32nd International Electric Propulsion Conference*, 2011, no. IEPC Paper 2011–217.

[24] M. L. R. Walker and A. D. Gallimore, "Neutral density map of Hall thruster plume expansion in a vacuum chamber," *Review of Scientific Instruments*, vol. 76, no. 5, p. 053509, 2005.

[25] S. Dushman and J. M. Lafferty, *Scientific Foundations of Vacuum Technique. Second Edition*. John Wiley & Sons Inc, 1962.

[26] C. McLean, J. McVey, and T. Schappell, "Testing of a U.S.-built HET system for orbit transfer applications," *35th Joint Propulsion Conference and Exhibit*, Jun. 1999.

[27] J. Snyder, J. Baldwin, J. D. Frieman, M. L. R. Walker, N. S. Hicks, K. A. Polzin, and J. T. Singleton, "Flow Control and Measurement in Electric Propulsion Systems: Towards an AIAA Reference Standard," in *Proceedings of the 33rd International Electric Propulsion Conference*, 2013, no. IEPC Paper 2013–425.

[28] J. Kurzyna, S. Mazouffre, A. Lazurenko, L. Albarel̀€de, G. Bonhomme, K. Makowski, M. Dudeck, and Z. Peradzynski, "Spectral analysis of Hall-effect thruster plasma oscillations based on the empirical mode decomposition," *Phys. Plasmas*, vol. 12, no. 12, p. 123506, 2005.

[29] A. Litvak, Y. Raitses, and N. Fisch, "Experimental Studies of High-Frequency Oscillations in Hall Thrusters," *38th AIAA/ASME/SAE/ASEE Joint Propulsion Conference & Exhibit*, Jul. 2002.

[30] K. G. Xu and M. L. R. Walker, "High-power, null-type, inverted pendulum thrust stand," *Review of Scientific Instruments*, vol. 80, no. 5, p. 055103, 2009.

[31] S. Absalamov, V. Andreev, T. Colbert, M. Day, V. Egorov, R. Gnizdor, H. Kaufman, V. Kim, A. Koriakin, and K. Kozubskii, “Measurement of plasma parameters in the Stationary Plasma Thruster (SPT-100) plume and its effect on spacecraft components,” 1992, no. AIAA-92–3156.
[32] L. B. King, “Transport-Property and Mass Spectral Measurements in the Plasma Exhaust Plume of a Hall-Effect Space Propulsion System,” Dept. of Aerospace Engineering, Univ. of Michigan, Ann Arbor, MI, 1998.
[33] K. G. Xu, “Ion Collimation and In-Channel Potential Shaping using In-Channel Electrodes for Hall Effect Thrusters,” Georgia Institute of Technology, 2012.

[34] Sheehan, J. P., and Hershkowitz, N. "Emissive probes," Plasma Sources Science and Technology Vol. 20, No. 6, 2011, p. 063001. doi: 10.1088/0963-0252/20/6/063001